Impact of Accurate Geoid Fields on Estimates of the Ocean Circulation

DETLEF STAMMER AND ARMIN KÖHL

Institut für Meereskunde, Zentrum für Meeres- und Klimaforschung, Universität Hamburg, Hamburg, Germany

CARL WUNSCH

Department of Earth, Atmospheric and Planetary Sciences, Massachusetts Institute of Technology, Cambridge, Massachusetts

(Manuscript received 12 December 2005, in final form 20 November 2006)

ABSTRACT

The impact of new geoid height models on estimates of the ocean circulation, now available from the Gravity Recovery and Climate Experiment (GRACE) spacecraft, is assessed, and the implications of far more accurate geoids, anticipated from the European Space Agency's (ESA) Gravity and Ocean Circulation Explorer (GOCE) mission, are explored. The study is based on several circulation estimates obtained over the period 1992–2002 by combining most of the available ocean datasets with a global general circulation model on a 1° horizontal grid and by exchanging only the EGM96 geoid model with two different geoid models available from GRACE. As compared to the EGM96-based solution, the GRACE geoid leads to an estimate of the ocean circulation that is more consistent with the Levitus temperature and salinity climatology. While not a formal proof, this finding supports the inference of a substantially improved GRACE geoid skill. However, oceanographic implications of the GRACE model are only modest compared to what can be obtained from ocean observations alone. To understand the extent to which this is merely a consequence of a not-optimally converged solution or if a much more accurate geoid field could in principle play a profound role in the ocean estimation procedure, an additional experiment was performed in which the geoid error was artificially reduced relative to all other datasets. Adjustments occur then in all elements of the ocean circulation, including 10% changes in the meridional overturning circulation and the corresponding meridional heat transport in the Atlantic. For an optimal use of new geoid fields, improved error information is required. The error budget of existing time-mean dynamic topography estimates may now be dominated by residual errors in time-mean altimetric corrections. Both these and the model errors need to be better understood before improved geoid estimates can be fully exploited. As is commonly found, the Southern Ocean is of particular concern.

1. Introduction

Global state estimation (data assimilation) has become a near-routine method for producing dynamically and statistically self-consistent syntheses of circulation models and oceanic data (Stammer et al. 2002a, 2003, 2004; Köhl et al. 2007; Wunsch and Heimbach 2006). Their methodology is a form of constrained least squares and, as in any least squares method aiming at a minimum variance estimate, one of the essential ingredients in carrying out such calculations is a quantitative description of the error structure of the data being used. Solutions that are forced closer to observations than is warranted are modeling noise; solutions not close enough to the observations are discarding useful information. Prior error information and residuals of all data types used in such calculations therefore have to be examined in great detail since any inconsistency carries important information about unaccounted data and/or model errors.

Here, we examine the time-mean dynamic topography component of the state estimates as used in the work of the Estimating the Circulation and Climate of the Ocean (ECCO) Consortium (Stammer et al. 2002b) and its German partner (GECCO). Our specific goals are threefold: 1) to determine the impact of the time-mean dynamic topography on the estimated solution; 2) to determine the impact of more accurate geoid fields on a hypothetically converged solution; and 3) to dis-

Corresponding author address: Detlef Stammer, Institut für Meereskunde, Zentrum für Meeres- und Klimaforschung, Universität Hamburg, Bunderstrasse 53, 20146 Hamburg, Germany.
E-mail: stammer@ifm.uni-hamburg.de

DOI: 10.1175/JTECH2044.1

cuss the error information of the dynamic topography required for such an enterprise, beyond just the geoid error covariance. The approach taken is to compare optimization results obtained by using the different geoids along with all of the other data going into the ECCO/GECCO estimates. The paper is an extension of a previous study by Köhl et al. (2007, hereafter KEA07). Those authors describe a first ECCO synthesis on a global 1° geographical grid for the period 1992 through 2002 that was carried out using the first geoid estimate derived from the Gravity Recovery and Climate Experiment (GRACE) geoid (Tapley et al. 2003). Subsequently, Wunsch and Heimbach (2006) carried that estimate forward through 2004.

This article can also be understood as an attempt to extend the previous analyses of the impact of improved geoid estimates on the problem of determining the ocean circulation (Ganachaud et al. 1997; LeGrand et al. 1998; Rio and Hernandez 2004; among others). These earlier papers focused, from practical necessity, on the nominally steady-state ocean circulation. Wunsch and Stammer (2003) then discussed the potential of ocean state estimates as consistency tests and highlighted that the combination of geodetic and oceanographic knowledge permits a better estimate of the geoid as well as the ocean circulation. Here we extend the previous discussion to a fully time-dependent system. As discussed below, we have progressed to the point where the lack of understanding of data and model errors seriously inhibit the possibility of making improved estimates of elements of the ocean circulation. Jayne (2006), in a study related to this one, studies the impact of the GRACE geoid on ocean circulation estimates, but confined to the North Atlantic.

2. Uncertainties in dynamic topography fields

Existing ECCO state estimation efforts are constrained by many data types and their respective error estimates. Among those is the time-mean surface dynamic topography, which is calculated as the difference between time-mean altimetric observations of the sea surface height (SSH) minus a geoid height model. Accordingly, the error covariance for the surface dynamic topography has to take into account errors in both the geoid and the altimetric observations. In the past, geoid uncertainties were considered to dominate the errors of the dynamic topography. However, with ever-decreasing geoid height errors, the uncertainties in the time-mean and time-varying altimetric data are gaining importance, to the point that they may already dominate the error budget of the surface dynamic topography field. Geoid height errors include commission and omission errors alike. The latter are significant on small spatial scales not resolved with a given degree/order, which are important for capturing energetic ocean circulation structures. Because of this effect, one has to smooth the model sea surface height so that it does not contain signals on scales smaller than available in a geoid model provided to a predescribed degree and order.

The other important contribution to the error of the dynamic surface topography comes from altimeter errors. Theses are often conveniently separated into those of the time-mean and those of the temporal anomalies. Unfortunately, the separation is not an absolute one, as the mean continues to be estimated over ever-increasing time intervals and there is no known frequency below which the time variations in the errors vanish. Chelton et al. (2001) summarize best estimates of the time-mean and total errors as of that time. According to their Table 11, the root-mean-square (RMS) altimetric errors are about 4 cm, but results suggest strong regional variations in this and the time-mean value, the latter perhaps reaching over 10 cm in the Southern Ocean (due to errors in wind and wave observations there). A definitive discussion is impossible at the present time, and the lack of proper information on the background time-mean altimetric error must be borne in mind in the following discussion of the geoid component.

An updated discussion of the time-variable errors was provided recently by Ponte et al. (2007). Their comparisons between the independent Ocean Topography Experiment (TOPEX)/Poseidon (T/P) and *Jason-1* altimetric missions, when they were in identical orbits, show that point-by-point, the data are consistent within the mission specifications of about 3-cm RMS error, but large-scale dependences exist in the data differences, and these are both poorly known and capable of introducing major errors into oceanic state estimates. The analysis reveals errors reaching 4 cm at mid- and high latitudes and lower ones present in low latitudes.

3. Methodology

Our methodology is to fit a general circulation model (GCM) to a very large set of regional and global data using constrained least squares. For this purpose, Lagrangian multipliers are used and the fit is an iterative one [see Wunsch (2006) for a summary]. The underlying model, data, and methodology are described by Stammer et al. (2002a, 2003). KEA07 describe in detail the specific model setup and datasets used as well as the optimization procedure and results.

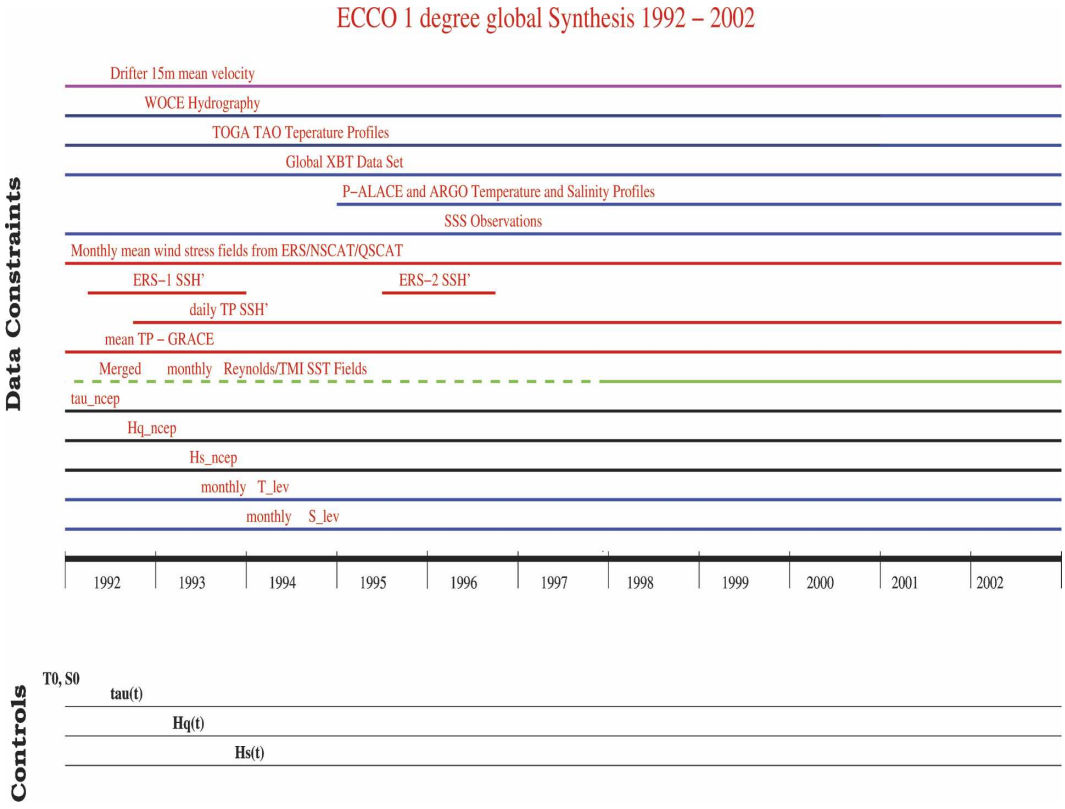

FIG. 1. Schematic of the optimization. (top) The data constraints imposed on the model during optimization 2 and optimization 3. The lines indicate times where data are available; mean or climatological data are shown as available throughout the whole period. (bottom) The "control variables" that were changed during the optimization.

In brief, the ECCO GCM is based on the Massachusetts Institute of Technology (MIT) GCM described by Adcroft et al. (2002), coupled to a surface mixed layer model (Large et al. 1994) and using the eddy parameterization scheme of Gent and McWilliams (1990). In our present experiments, the horizontal model resolution is 1° over ±80° in latitude with 23 levels in the vertical, and the estimation period covers the years 1992 through 2002. In experiment *optimization* 2, the difference T/P − GRACE − University of Texas GRACE geoid model (GGM01c; Tapley et al. 2003) was used to constrain the time-mean dynamic surface topography, using a spatially uniform error of 4.5 cm. A schematic of the data constraints is displayed in Fig. 1; they include several satellite datasets [altimetry from T/P, European Remote Sensing Satellites (*ERS-1* and *-2*), scatterometer data, and Reynolds and microwave SST fields], time-mean surface drifter velocities, in situ hydrographic temperature and salinity profiles, as well as hydrographic sections.

In an earlier calculation (called *optimization* 1 hereafter), the difference T/P minus the EGM96 geoid (Lemoine et al. 1997) was used to impose constraints on the time-average absolute circulation (see Köhl et al. 2002). A diagonal covariance matrix was used with values taken from the diagonal of the EGM96 error covariance matrix (cf. Lu et al. 2002). An estimate of the resulting 11-yr time-mean dynamic topography field is displayed in Fig. 2a. On the large scale, the results resemble the observed dynamic topography associated with the basin-scale gyre structure of the ocean. However, differences on subbasin scales loom large. Figure 2b shows the associated residuals relative to the imposed mean dynamic topography of the combined missions (data are all T/P) in the model referred to in EGM96. Values are on the order of ±20 cm and reach ±50 cm near steep topography. These differences contradict the estimated prior geoid error fields and a goal here is to understand those residuals in terms of model and data errors alike. For that purpose, the combination of optimization 1 and optimization 2 is used to investigate the following question: does the near-optimized model fit better to the time-mean altimetry based on GRACE than it does to EGM96 assuming

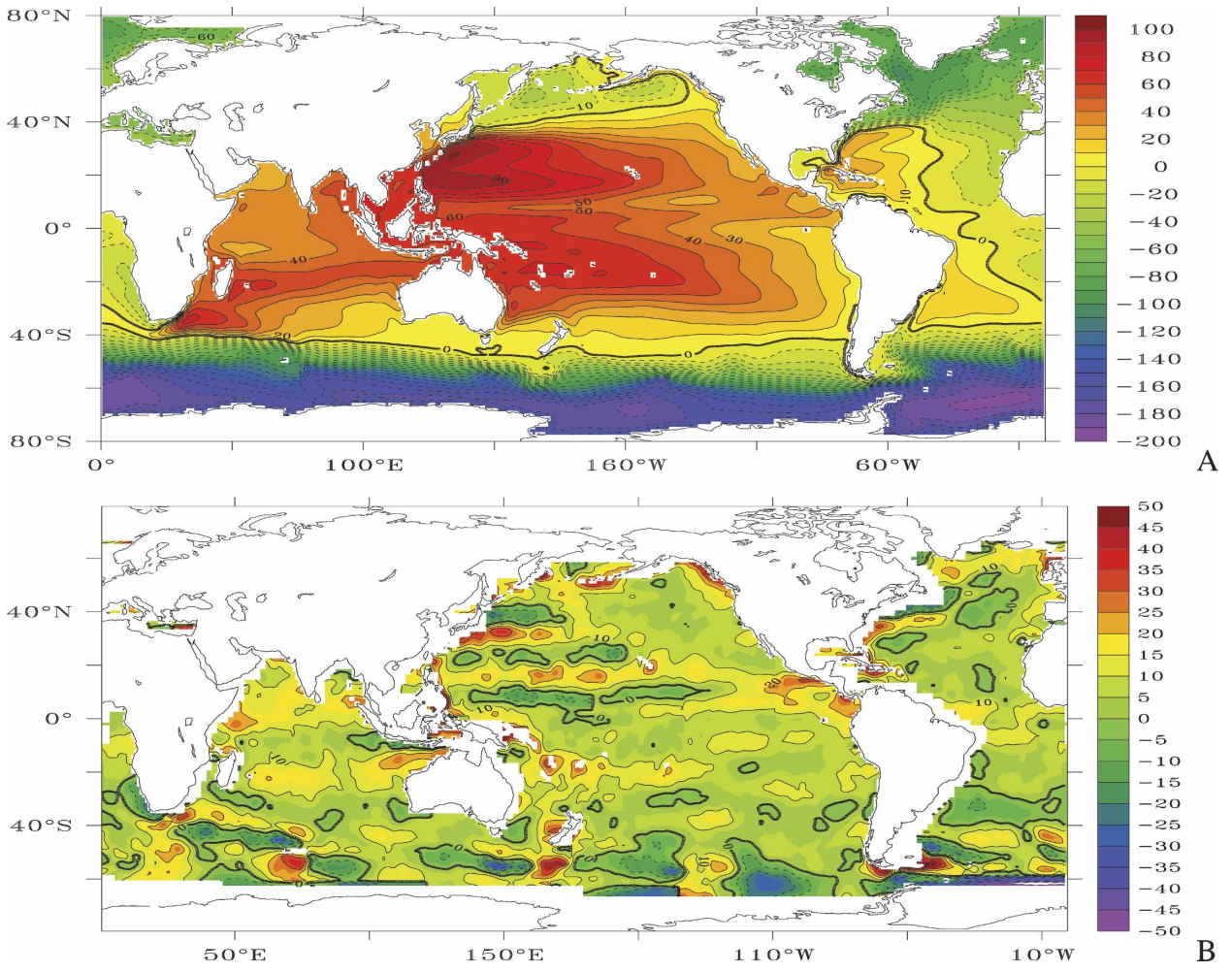

FIG. 2. (top) Time-mean sea surface height (dynamic topography) as it results from the 11-yr-long optimization 2. (bottom) Optimized dynamic topography differences with respect to T/P − EGM96. Contour interval is 10 cm. This field can be regarded as an ECCO-computed adjustment to the geoid to render it consistent with the model and other data.

that the GRACE error estimates are approximately correct?

In experiment *optimization* 3, we then used the difference T/P − GRACE − GGM02C (Tapley et al. 2005) as a constraint on the time-mean dynamic surface topography, but with an artificially increased accuracy for the mean dynamic topography field. The combination of optimization 1 and optimization 3 will be used to address the question raised by Ganachaud et al. (1997) of the extent to which a *much* improved geoid estimate would carry information about the ocean circulation not already contained in other data and in the model physics themselves. While we force the model very strongly toward the GRACE-based dynamic topography, resulting inconsistencies with prior in situ and geoid data—or the lack thereof—will permit the determination of whether the new solution is plausible or not.

4. Impact of the GRACE geoid

To investigate the reason for the large SSH residuals relative to the EGM96-based dynamic topography, optimization 2 was performed in which all constraints remain the same except that the time-mean T/P dynamic topography field minus GGM01c was imposed over the entire 11-yr period. As advised by GRACE, a geographically uniform error value of 4.5 cm was employed along the covariance matrix diagonal. In simple terms, this error can be understood as being composed of roughly 3-cm RMS GRACE error plus 3.5-cm RMS mean T/P time-mean error (the latter is very optimistic, especially over the Southern Ocean as discussed above, but only the sum of the errors affects the results). Optimization 2 was run in parallel to the last six iterations of optimization 1.

Figure 3a shows the contributions to the total objec-

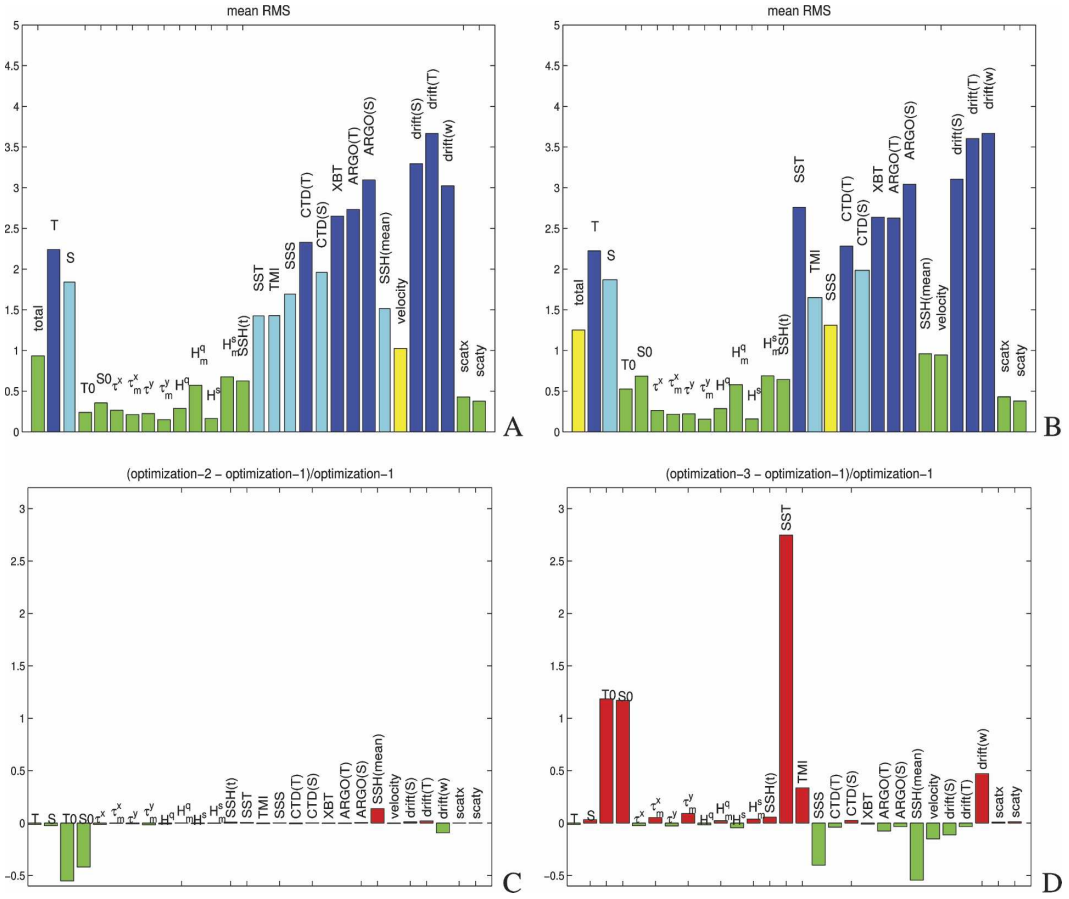

FIG. 3. (top) Objective function contributions from individual datasets for the optimized state taken from (left) optimization 2 and (right) optimization 3. Bars represent values for the optimized state after normalization with the number of observations. The labels "T" and "S" describe the Levitus terms followed by the initial conditions "TO" and "SO"; "τ^x," "τ^y," "H^q," and "H^s" correspond to zonal and meridional wind stress, heat flux, and freshwater flux corrections (the subscript m indicates the mean), respectively. "Drift(T)," "drift(S)," and "drift(w)" are the drift terms as described in the main text; "scatx" and "scaty" correspond to zonal and meridional scatterometer wind stress data, and "velocity" to the mean velocity field from the drifter data. Other labels stand for the data type. See Table 1 for more details. (bottom) The changes of each bar (left) between optimization 2 and optimization 1 and (right) between optimization 2 and optimization 1, both normalized by values of optimization 1. Negative values indicate a fractional improvement in the quadratic model data misfit for each variable.

tive (or misfit or cost) function that result from individual datasets and remain as residuals at the end of the experiment optimization 2. Each column is labeled according to the dataset it represents as explained in detail in the figure caption and in Table 1. Each column was normalized by the corresponding number of data points used as constraints and divided by the prior error variance; the square root is taken subsequently for plotting. In this form, a fully converged solution would have an expected value of one for which each column and misfits would be distributed in a χ^2 distribution without spatial structures. The figure reveals that the total misfit is close to the ideal number of one but that the solution is not yet fully converged in the sense that individual columns do deviate from the ideal value of 1. The same holds for optimization 1 and optimization 3 as well. An alternative interpretation could be that prior error statistics are not compatible with the model and the data—a subject of ongoing research. Nevertheless, large-scale features in the estimate appear to be relatively insensitive to the continuing slow improvements established during additional iterations, allowing the use of the existing solutions for the present investigation.

Figure 3c shows the fractional changes in the RMS model data misfits of optimization 2 minus the results from optimization 1 normalized by results from optimization 1; that is, negative numbers in the figure indicate

TABLE 1. Components of the cost function displayed in Fig. 3.

Column	Label	Variable
1	Total	Total model data misfit
2	T	Monthly mean Levitus temperature, top to bottom
3	S	Monthly mean Levitus salinity, top to bottom
4	T_0	Changes of initial temperature conditions relative to Levitus January
5	S_0	Changes of initial salinity conditions relative to Levitus January
6	τ^x	Changes in zonal wind stress anomalies
7	τ^x_m	Changes in time-mean zonal wind stress
8	τ^y	Changes in the prior meridional wind stress anomalies
9	τ^y_m	Changes in the prior time-mean meridional wind stress
10	H^q	Changes in the prior surface heat flux anomalies
11	H^q_m	Changes in the prior time-mean surface heat flux
12	H^S	Changes in the prior surface salt flux anomalies
13	H^S_m	Changes in the prior time-mean surface salt flux
14	SSH(t)	Misfit to the T/P and ERS SSH anomalies
15	SST	Misfit to Reynolds and Smith (1994) SST fields
16	TMI	Misfit to TMI SST fields
17	SSS	Misfit to SSS observations
18	CTD(T)	Misfit to CTD temperature profiles
19	CTD(S)	Misfit to CTD salinity profiles
20	XBT	Misfit to XBT temperature profiles
21	ARGO(T)	Misfit to ARGO temperature profiles
22	ARGO(S)	Misfit to ARGO salinity profiles
23	SSH(mean)	Misfit to the T/P–geoid mean dynamic topography
24	Velocity	Misfit of the 15-m time-mean velocity field to time-mean drifter velocities
25	Drift(S)	Difference of the last year minus first year salt differences
26	Drift(T)	Difference of the last year minus first year temperature differences
27	Drift(w)	Difference of the last year minus first year vertical velocity differences
28	Scatx	Misfit to scatterometer zonal wind stress observations
29	Scaty	Misfit to scatterometer meridional wind stress observations

the fractional improvements in the model data misfits imposed through the use of the GRACE geoid height. From the figure it follows that

1) Replacing EGM96 by the GRACE geoid model and reducing the squared error of the dynamic topography to $(4.5\ \text{cm})^2$ while leaving all other optimization parameters unchanged produces a new solution with its initial conditions significantly closer to the Levitus and Boyer (1994) and Levitus et al. (1994) climatological temperature (T) and salinity (S) fields. This result can be seen from columns 3 and 4 of Fig. 3c, showing up to 50% less deviations from the Levitus temperature and salinity fields than were found in optimization 1. This improvement could be a coincidence because the climatology itself has large and poorly understood errors (see, e.g., Forget and Wunsch 2007). However, it also suggests that the T/P–GRACE dynamic topography is more in line with estimates based on in situ data.
2) Because of the smaller adjustment to Levitus initial temperature and salinity conditions, the model also stays dynamically more balanced, as suggested by the reduction in the vertical velocity drift during optimization 2, as can be seen from the third to last column of Fig. 3c. Misfits between the monthly mean climatological hydrographic fields from optimization 2 and climatological fields are also slightly smaller (columns 1 and 2 of Fig. 3c). Again, both can be interpreted as indications of a dynamically more consistent T/P–GGM01c dynamic topography (i.e., more skill in the GRACE geoid field).
3) The time-mean misfit of the dynamic topography increases with the use of the GRACE geoid. This increase is primarily due to the reduced prior error of the new geoid (i.e., because the misfit terms are divided by a smaller number). Nonetheless, the absolute (unweighted) misfit decreases as demonstrated in Fig. 4a.

These residuals are much smaller than those found from the differences of optimization 1 from the EGM96-based SSH field (cf. Fig. 2b). The dynamic topography misfit in optimization 2 now shows residuals on the order of ± 10 cm but still reaches ± 40 cm on relatively short spatial scales near steep topography, especially over the Southern Ocean. The implication is that the 4.5-cm RMS error for the time-mean dynamic

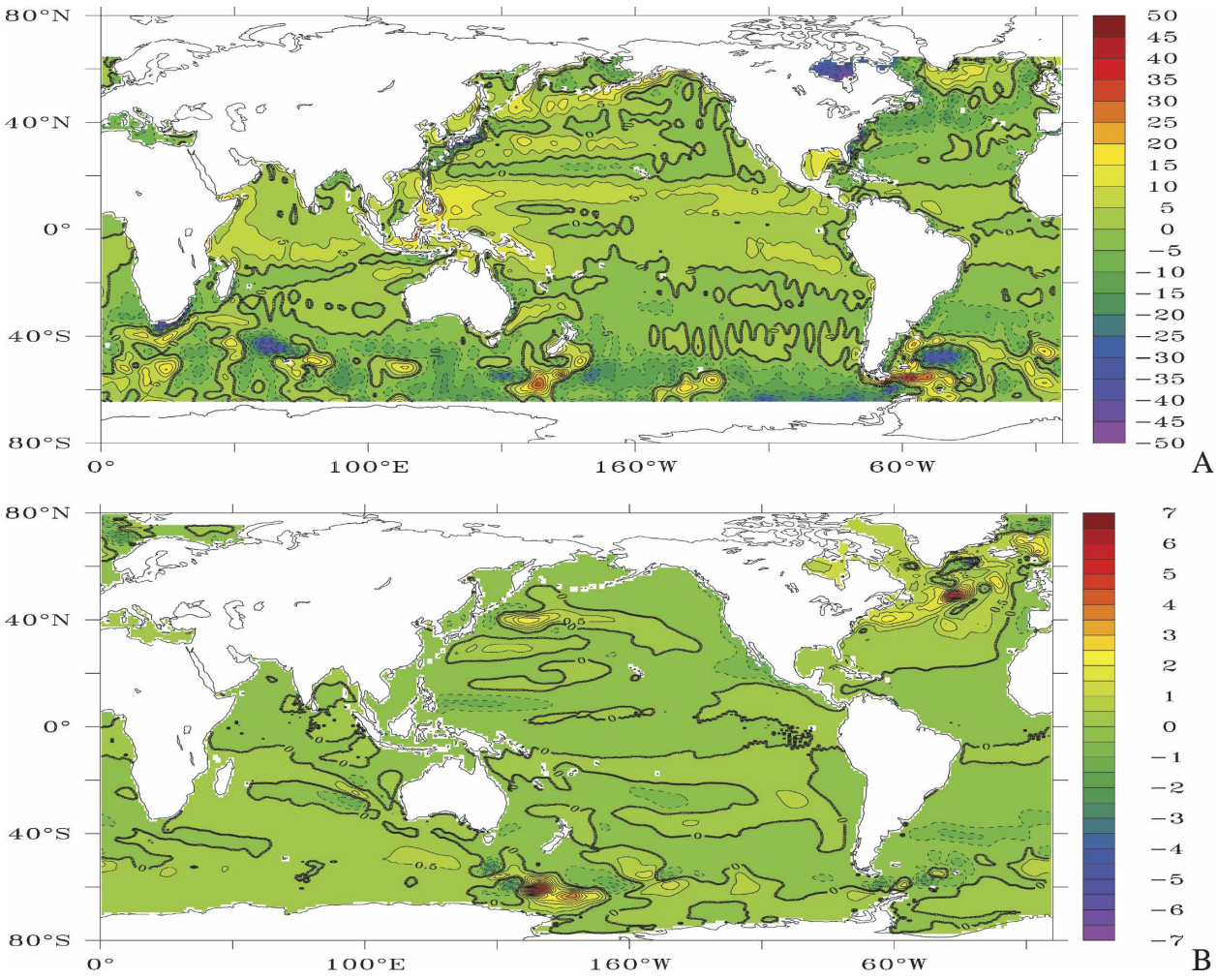

FIG. 4. Differences in the time-mean dynamic topography (cm) between (top) optimization 2 and the T/P–GGM01c and (bottom) optimization 2 and optimization 1.

topography remains unrealistically optimistic in those regions and that a full error covariance budget for the dynamic sea surface height is required—one that would have strong spatial variability and accounts for commission and omission errors in the geoid and errors in the T/P data and the model. It will be very important to analyze in detail the residuals between the GRACE-based dynamic topography and the model results work that is underway currently and which also needs to address model errors in detail.

Figure 4b, showing the differences in the estimated time-mean dynamic topography obtained from optimization 2 minus that of optimization 1, illustrates that adjustments in the dynamic topography forced in optimization 2 relative to those in optimization 1 are small. Large-scale changes are typically only on the order of 1 cm or less and arise from changes in temperature and salinity (not shown) on the order of ±1° and ±0.1 psu, respectively (depending on the depth), bringing the second optimization closer to the hydrographic climatology. Maximum differences of ±5 cm are reached only in two regions.

Two implications follow from the figure: 1) the previous solution was not significantly overconstrained by the errors in the EGM96 model. Only in a few places the GRACE-based SSH solution moves away from it, notably in the Southern Ocean south of New Zealand, in the western North Pacific north of the Kuroshio Extension, and in the subpolar North Atlantic. Adjustments in all other regions are only minor; and 2) because of those small overall changes in SSH, no additional knowledge about the ocean circulation or ocean transports was extracted from the new GRACE geoid field relative to what we know from in situ and altimeter data.

Goals of ocean state estimation include the identifi-

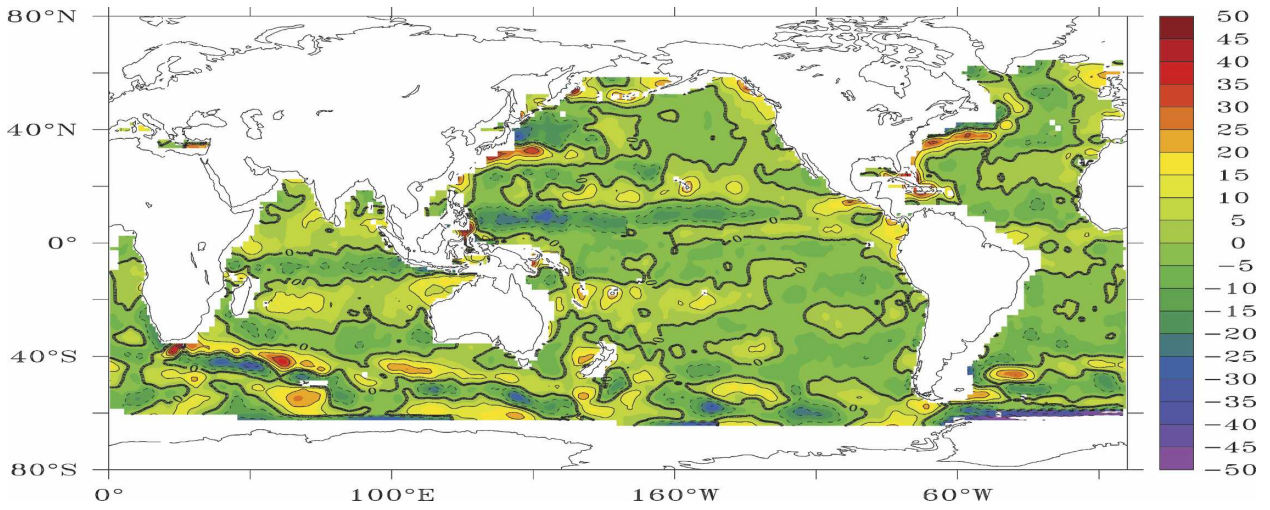

FIG. 5. Differences between the GGM02c and the EGM96 geoid models.

cation of inconsistencies in the geoid model and its prior error description (like with any other dataset) and to help improve them. Can we identify EGM96 errors from the existing optimizations (i.e., can the residuals, shown in Fig. 2b, be identified as uncertainties in the EGM96 geoid model)? To some level this question can be addressed by investigating the differences between the EGM96 and the hypothetically much more accurate GRACE geoid models, shown in Fig. 5. A visual inspection reveals that many of the structures shown in Fig. 2b are actually also present in the geoid difference field with comparable amplitude. The figure therefore suggests that a significant fraction of the SSH misfit obtained from optimization 1 represents uncertainties in the EGM96 geoid model not accounted for by its error variance and that the ocean state estimation procedure provided additional information for the improvement of this geoid model, except it so far does not provide a full geoid error covariance matrix.

One might wonder if we can also interpret the residuals resulting from optimization 2 (Fig. 4) as uncertainties in the GGM01c model by comparing the two GRACE geoid models GGM01c and GGM02c. However, differences between those two solutions reside to first order on small spatial scales and do not resemble the residuals we encounter in optimization 2. To answer the above question to what extent Fig. 4 resembles GGM01c errors or if, rather, residuals reveal T/P or model errors would need to await the new Gravity and Ocean Circulation Explorer (GOCE) geoid, which is supposed to be a much more accurate geoid than GRACE on scales relevant for basin-scale and regional ocean circulation. Until then, ocean information has to be used to answer this question.

5. Impact of a hypothetically accurate GOCE geoid

We have seen that the impact of a new GRACE geoid on the ocean state estimate is quite small and does not lead to a significant modification of the previous ocean circulation solution. However, because the underlying state estimate is not yet fully converged in the sense that all model data residuals diminished to statistically acceptable levels implies that the contribution of the misfit of the mean dynamic topography to the total cost function remains relatively small and therefore relatively insignificant. The question therefore arises if this is so because the information content in the geoid relative to other ocean data is comparatively low as suggested by Ganachaud et al. (1997) and LeGrand et al. (1998), or whether it is merely the consequence of the failure to bring the system to the asymptotic, fully optimized state (i.e., all misfit terms are much larger than a final state would warrant, or whether the failure to take model errors properly into account poses a principal problem with the given optimization setup, e.g., spatial resolution).

In an attempt to investigate these possibilities, optimization 2 was continued as optimization 3 after replacing GGM01c with GGM02c, with the geoid height error kept fixed, but now with the weights of all remaining misfit terms reduced significantly to simulate a converged solution for which then the mean dynamic topography based on new geoid models can make a sizable contribution to the cost function. To this end, we artificially force the model to the time-mean dynamic topography by increasing the relative errors on the nongeoid misfit terms by a factor of 12 during 10 further

iterations, and then by a factor of 50 during a final 9 iterations.

Resulting contributions to the objective function are displayed in Fig. 3b. To compare this figure with results from optimization 2, we use the error weights of optimization 2 in both Figs. 3a and 3b. Figure 3d shows changes in the RMS misfits of optimization 3 minus the results from optimization 1, again normalized by optimization 1. Under present circumstances, we observe a clear decrease of the misfit in the time mean SSH by 50%. But as compared to optimization 2, complex adjustments take place in the absolute misfits of the remaining data to accomplish this success. For example, there is improvement and degradation of monthly mean temperature and salinity misfits (by a few percent), averaging nearly to zero (columns 1 and 2). Sea surface salinity (SSS) misfits are improved (column 16), but SST degrades (column 14). Also noteworthy is the substantial increase in the misfit of the initial temperature and salinity conditions relative to the hydrographic climatology, as well as the drift term in the vertical velocity measuring the dynamical imbalance of the initial conditions. We also note a slight increase in the misfit of all time-mean forcing fields from the NCEP first-guess conditions. While overall the misfit of time-mean components increases, most of the residuals in time-varying datasets diminish. This is especially true for the misfits to all vertical profile data, such as expendable bathythermographs (XBTs), ARGO, and CTD data.

All these changes are difficult to interpret, as they depend upon the detailed nature of the real errors in the GRACE geoid as well as inaccuracies in the remaining data types, neither of which are well known. In the following we will first discuss changes in control terms and discuss their consistency with prior information. We will subsequently analyze changes in the flow field imposed by the geoid field and the associated changes in the control terms.

a. Changes in control terms

Figure 3d indicates that overall changes to initial conditions of temperature and salinity relative to the Levitus fields are significantly enhanced in optimization 3, as are associated amplitudes in the vertical velocity during the first year. An inspection of the fields reveals, however, that this does not hold throughout the model domain, but that it is actually limited to the abyssal Antarctic Circumpolar Current (ACC) region. To illustrate the changes occurring there, the top and bottom panels of Fig. 6 show a section along 60°S of the changes in temperature and salinity initial conditions, respectively. Most noticeable are changes directly adjacent to strong topographic slopes, which suggest that the interaction with bottom topography is the main agent bringing the model into consistency with the new mean dynamic topography field, locally and upstream (westward). Amplitudes of the adjustments are on the order of 0.5°C and 0.5 psu in salinity, even at 3000-m depth. While those changes appear unreasonably high, we have to recall that the Southern Ocean is not properly sampled in the hydrographic climatology fields and that local errors in the hydrographic fields are likely to be significantly larger than what would seem acceptable (e.g., for the North Atlantic). As a result, the solution cannot be rejected as entirely implausible (see also below). Nevertheless, the Southern Ocean is a region of complex topography–flow interaction that to some extent takes place on small spatial scales not resolved in the present model solution (Olbers et al. 2004). Model errors are therefore likely to be especially important here. Finally, because of small-scale ridge structures having a strong imprint in the geoid field, omission errors should play a significant role in the Southern Ocean, like nearly all regions with complex bottom topography structures. An improved understanding of model errors and errors in the geoid field and altimeter data is therefore required to increase our understanding of the skill of estimation results in this region.

The remaining control parameters are the time-varying surface forcing fields of net heat and freshwater fluxes and wind stress. Figure 7 shows the time-mean changes in surface forcing fields between optimization 3 and optimization 1. Peak changes in estimated heat flux, freshwater flux, and wind stress are 14 W m^{-2}, 0.03 m yr^{-1}, and 0.005 N m^{-2}, respectively. We note that all those changes are well within prior error bars of the surface flux fields, even over the Southern Ocean.

In essence, some changes in the surface forcing fields confirm previous estimates described in detail by Stammer et al. (2004). Although changes in heating and freshwater fluxes tend to oppose each other in the density field, heat flux changes dominate by an order of magnitude. The largest adjustments occur along major current systems, including the Kuroshio, Gulf Stream, and ACC where amplitudes of flux fields and uncertainties are also large. Estimated changes of the zonal wind stress relative to the NCEP first guess in part enhance the changes made previously in optimization 1, but include also some new elements, especially in the Indian and Pacific Oceans. Without giving significance to specific state and adjustment, we conclude that a high-accuracy geoid, combined with the full error covariance of the dynamic topography, would provide information about the deep-ocean hydrography and

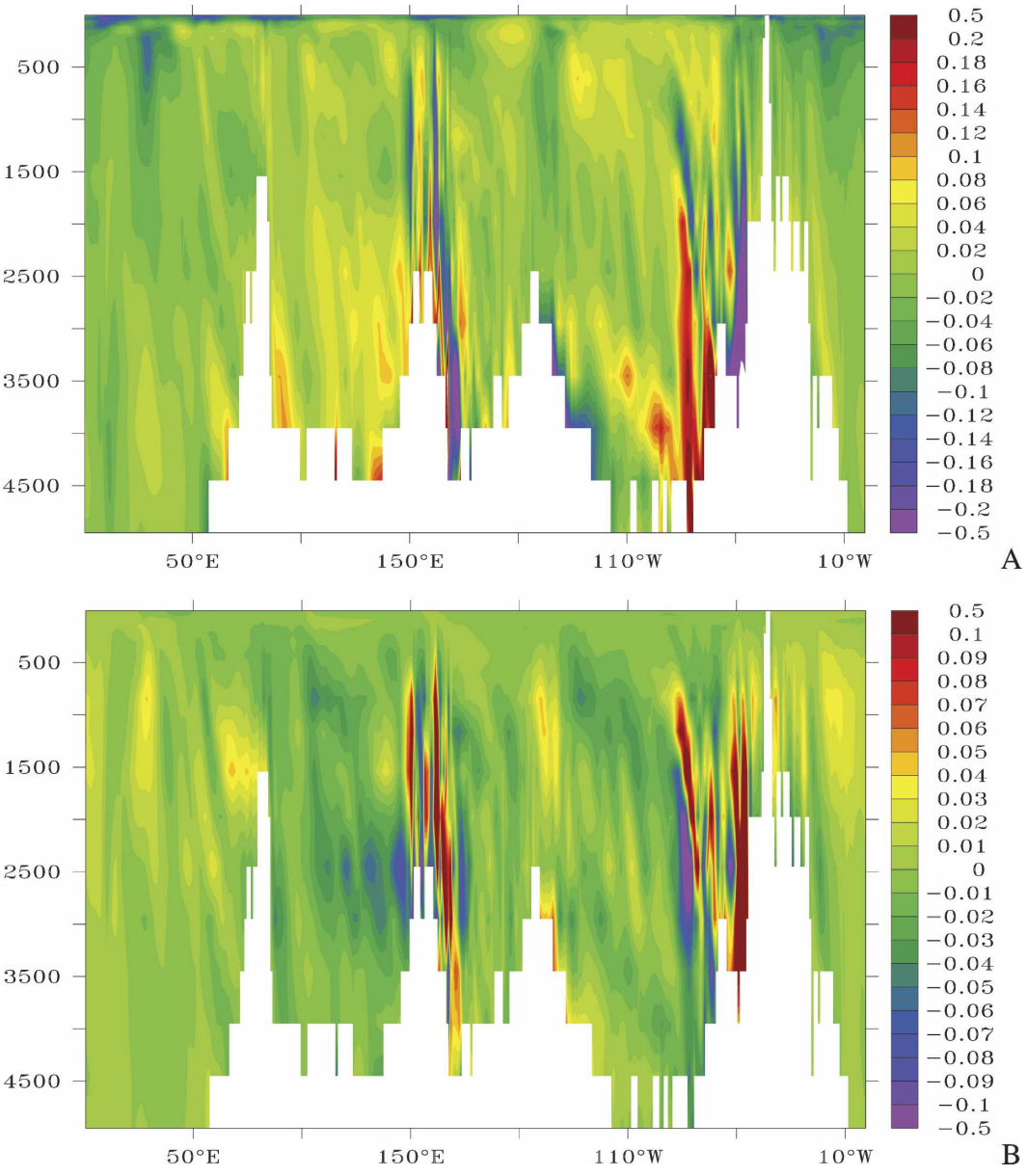

FIG. 6. Changes to the (top) initial conditions in temperature (°C) and (bottom) salinity (on the practical salinity scale) along 60°S.

about oceanic surface boundary conditions. Results shown here in essence illustrate the impact on meteorological estimates that could be expected from better geoid and dynamic topography fields.

b. Circulation changes

Figure 8 shows the dynamic topography residual before and after optimization 3 relative to the T/P–GGM02C geoid model. Differences diminish from the order of 10 cm to, typically, a few centimeters, with only the modest cost of control changes. The figure shows that increasing the relative weight of the time-mean dynamic topography leads to a significantly changed time-mean dynamic topography estimate. Although larger-scale gyre structures are adjusted, residuals remain on small spatial scales along boundaries, as expected given the absence of those scales in the geoid height estimate (omission errors). Differences also persist throughout the ACC, whereas the large-scale background of the dynamic topography model-data difference is removed, and only the chain of positive anomalies of positive anomalies, though reduced, remain.

Changes in the flow field enforced through the stronger geoid weighting are demonstrated in Fig. 9 in the

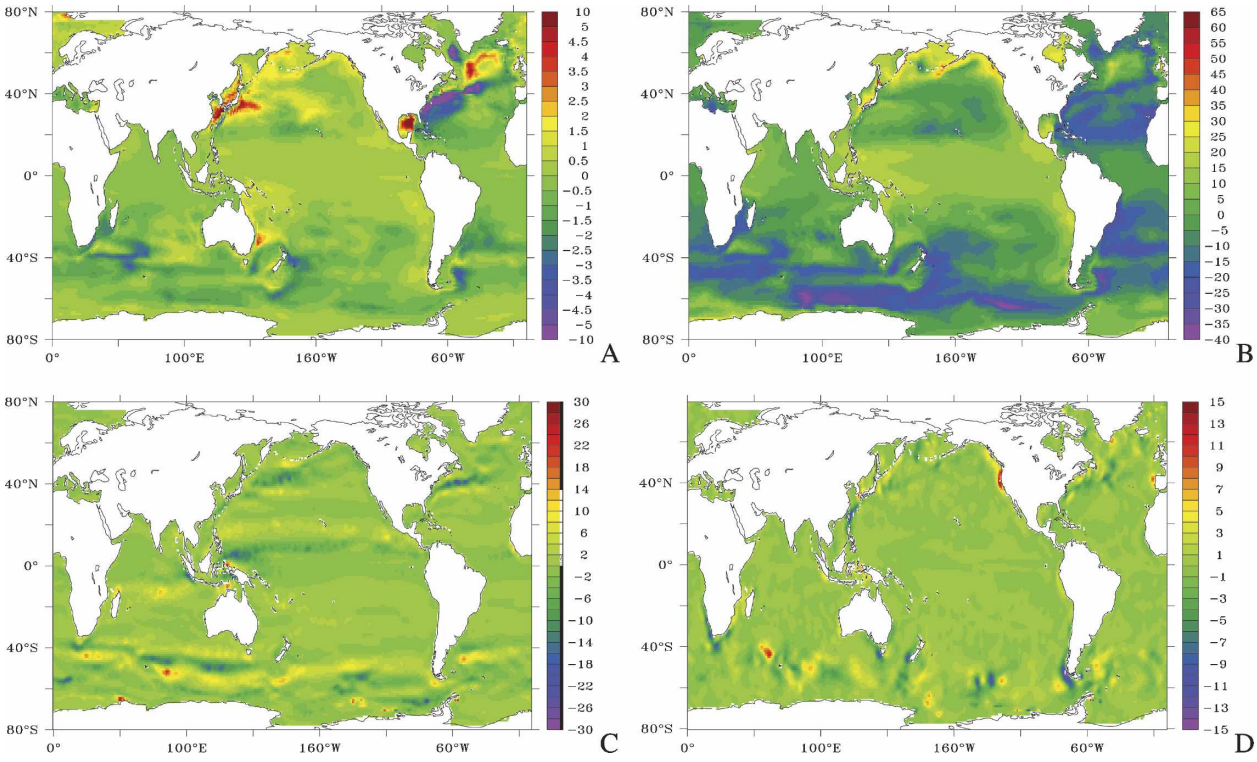

FIG. 7. Differences in the forcing corrections between optimization 3 and optimization 1. Shown are the (top left) time-mean heat flux corrections (W m^{-2}), (top right) time-mean freshwater flux corrections (mm yr^{-1}), and the time-mean adjustments to (bottom left) zonal and (bottom right) meridional wind stress in mN m^{-2}.

form of differences in the time-mean dynamic topography estimates between optimization 3 and optimization 1. Changes are now on the order of ±10 cm. Maximum amplitudes occur in the western tropical Pacific, the North Pacific, the subtropical and subpolar North Atlantic, and along the ACC. We note especially the adjustments occurring in the western North Atlantic where the new solution leads to an enhanced gyre transport and thus stronger North Atlantic Current. At the same time we find a depressed (i.e., stronger) subpolar gyre. In the North Pacific, many of the large-scale gyre structures are altered on a large zonal scale, indicating a basin-scale adjustment of the flow field, which in its tendency mirrors those changes described for the North Atlantic. Changes in the Southern Ocean essentially follow the path of the ACC in that the poleward side is being lifted (i.e., the current itself is being slightly decelerated in the Indian and Pacific sectors). We also note the relatively strong adjustments of SSH in the tropical oceans. Changes in time-mean temperature and salinity (not shown) are greatest near the surface, but they also have large vertical extent in the subpolar gyre. Differences in the flow field indicate a clear vertical coherence and are quite pronounced in the ACC and in the subpolar North Atlantic (on the order of 3 cm s^{-1}). Maximum changes are on the order of 3 and 1 cm s^{-1} in amplitude. The velocity pattern indicates a northward shift of the Gulf Stream and weaker slope water flow in optimization 3 near the surface.

In its lower panel, the figure shows changes in the barotropic stream function. Regionally, changes are on the order of ±5 Sv (1 Sv ≡ 10^6 m^3 s^{-1}) (e.g., in the North Atlantic). Drake Passage transports diminish by 4 Sv. Further details are provided in Table 2. All these changes have measurable consequences for transports, for example, changes imposed by the new geoid produce a weaker meridional overturning circulation (MOC) in the upper North Atlantic deep-water branch for optimization 3 relative to optimization 1 (by about 2 Sv; or about 10% of the mean value) (Fig. 10a). However, the deep cell (below 2000 m) is enhanced in the North Atlantic and decreased in the South Atlantic. In the lower panel, Fig. 10 shows the changes in the time-mean global meridional heat transport. Like MOC changes, maximum heat transport changes occur in the Southern Hemisphere, where increased southward (poleward) heat transport by up to 0.05 PW can be observed. Contributions from each of the oceans are of the same order but compensate each other partly. Again changes are on the order of 10% of the local time

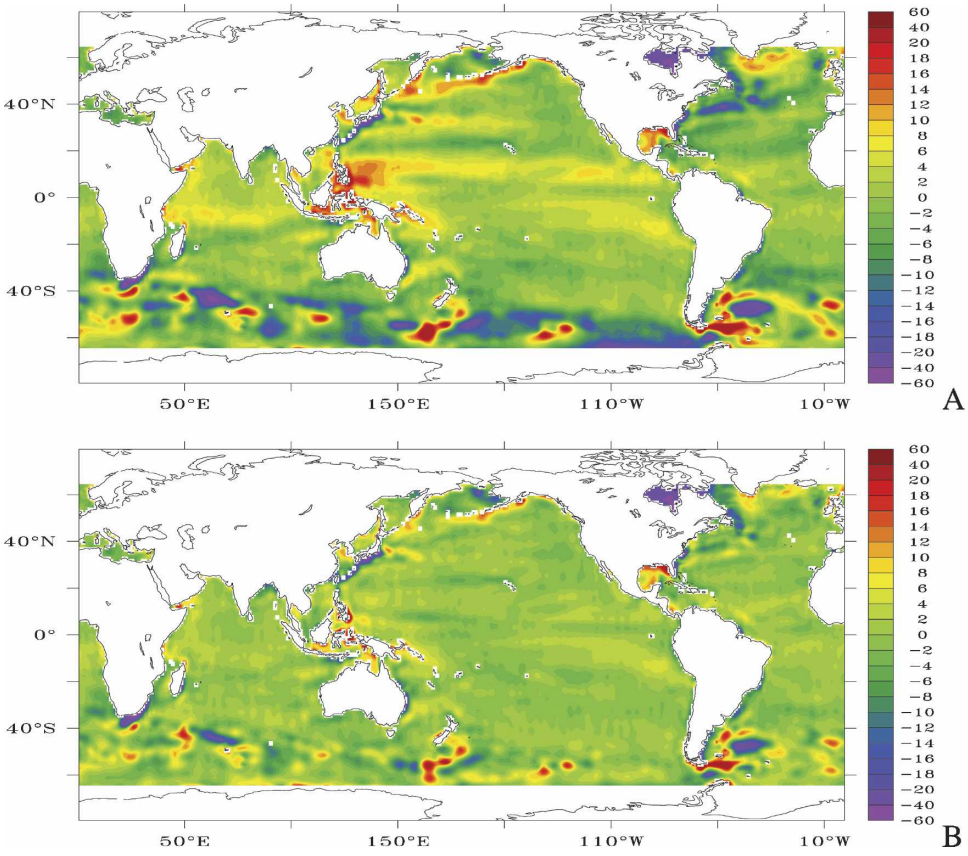

FIG. 8. Differences in the time-mean dynamic topography (cm) between (top) optimization 2 and the T/P–GGM02c and (bottom) optimization 3 and T/P–GGM02c.

mean value and as such are significant and of the same amplitude as climate variability.

All changes are oceanographically important, and it is important to be aware that carrying the optimization further would likely lead to even larger changes, although due to specific experimental setting, we do not attach any significance to specific changes. As with the control terms, the main information lies, instead, with the estimates of the magnitudes of the inferred changes, rather than with the spatial specifics.

6. Discussion

The comparison of the oceanographic implications of the EGM96 versus GRACE geoids for estimates of the ocean circulation supports the inference that the GRACE geoid has a significantly improved skill (as compared to EGM96) on spatial scales of 500 km and larger, implying that the GRACE geoid is closer to dynamical consistency with the GCM and other data than is EGM96. Our conclusion therefore is similar to the recent results from Birol et al. (2005) in that existing geoids do show skill in improving ocean circulation estimates on the large scale.

The apparent improvement has oceanographic and climate consequences consistent with the earlier inferences based upon steady-state assumptions. In particular, the GRACE geoid appears to be more consistent with temperature and salinity climatologies than is the older geoid, although this improvement is only weak and not definitive, given issues concerning the climatology accuracies. Nevertheless, the new geoid requires smaller adjustments to the initial model temperature and salinity conditions (from Levitus and Boyer 1994; Levitus et al. 1994). Although at present levels of accuracy, the GRACE geoid height estimates, while apparently an improvement over EGM96, do not lead to qualitative adjustment in the estimated ocean circulation, the optimization itself produces a new, and presumably, improved geoid estimate, but its full use requires an estimated error covariance, which is not yet available.

The implications of a much improved geoid (beyond that now available from GRACE) on a converged so-

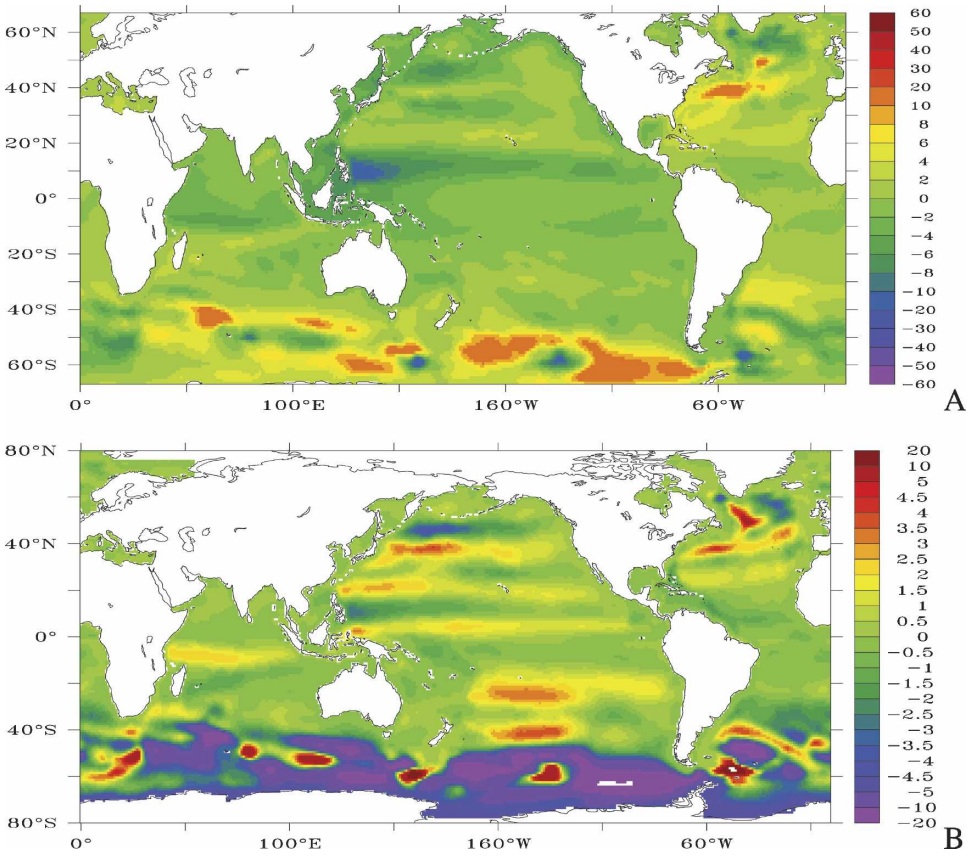

FIG. 9. (top) Differences in the time-mean dynamic topography (cm) between optimization 3 and optimization 1; (bottom) differences in the barotropic streamfunction between optimization 3 and optimization 1 (units: Sv).

lution can be explored by driving the model arbitrarily close to the existing geoid. Forcing such a fit produces structures in the inferred ocean circulation that are significantly different from those estimated using a realistic error estimate. This fit requires only small changes in the meteorological fields—ones that stay well within their error bars. The only region with unreasonable changes in control terms appears to be the Southern Ocean (besides boundary regions). There is no physical reason to reject these circulation structures over all other regions—they are meteorologically and oceanographically reasonable at the current levels of in situ observational error. However, there is no obvious independent test of their reality available. We seemingly have reached a stage with combined altimetry/geodesy in which further geoid improvement could significantly improve estimates of the ocean circulation. Whether such further improvement relative to the errors of the other data types is possible is unclear at the present time.

Because of the specifics of the experimental setup, we cannot attach any significance to specific adjust-

TABLE 2. Volume and enthalpy [with reference to 0°C in order to enable comparison with Ganachaud and Wunsch (2000)] transports through channels and passages as they follow from optimization 3 and optimization 1.

	Optimization 3		Optimization 1	
Location	Volume transport (Sv)	Heat transport (PW)	Volume transport (Sv)	Heat transport (PW)
Indonesian Throughflow	10.70	−0.91	10.73	−0.92
Drake Passage	150.1	1.53	154.8	1.58
Florida Straight	29.95	2.10	30.33	2.17
Madagascar Channel	−13.65	−0.86	12.96	−0.81
Denmark Straight	−5.04	0.00	−5.19	0.00

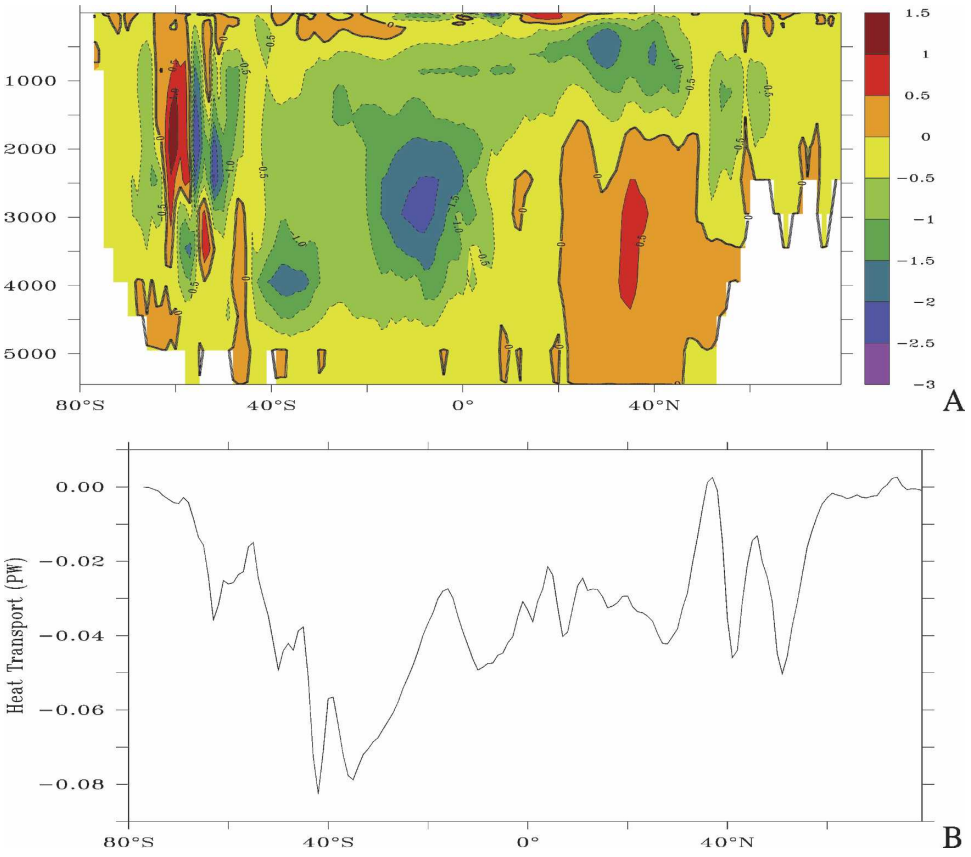

FIG. 10. (top) Differences in the global MOC (Sv) and (bottom) the global meridional heat transport (PW) between optimization 3 and optimization 1.

ments of the estimated circulation (i.e., we do not attach any significance to each detail in the changes because none of the solutions are fully converged). Rather, the main results lie with the estimates of the magnitudes of the inferred changes and their relation to prior information. In essence, the implications of this experiment are that if the accuracy of the GRACE-based dynamic surface topography were significantly better than now estimated, that quantitatively improved ocean circulation estimates would be obtained. If one simply assumed that the present GRACE geoid estimate were much more accurate than its authors believe, testing of the result would confront parallel and existing questions about the accuracy of the other data types (e.g., Forget and Wunsch 2007, for hydrographic data errors). However, remaining residuals near the boundaries and in the ACC indicate, particularly, the continued importance of the omission errors of the GRACE geoid—the missing short scales—as well as model uncertainties. But it may prove possible (e.g., Wunsch and Stammer 2003) to test the integral properties of such solutions against observations of the earth's rotation and polar motion in conjunction with adequate atmospheric models. It will be difficult but critical to confirm estimated changes in the circulation by independent means such as ocean time series or other independent in situ data.

However, for an optimal use of future precise geoids, improved error information is required. The error budget of existing time-mean dynamic topography estimates may now be dominated by residual errors in time-mean altimetric corrections and these need to be better understood jointly with model errors before present and future geoid estimates can be fully used in ocean studies, especially in the Southern Ocean. A critical issue remains in the need to better discriminate between errors in the altimetric and geoid estimates, neither of which are well understood at the levels of accuracy now apparently being achieved by ECCO-like estimation procedures. The results here suggest that a spatially uniform error in the existing GRACE geoid, as provided by the project, is qualitatively incorrect in many locations. As discussed above, the many elements of the altimetric error also appear to have strong spatial variability and the separation of time-mean and time-varying errors remains incomplete. As the measure-

ment errors decrease, we have to think about including model errors when assimilating mean SSH data.

Acknowledgments. Discussions with R. Ponte were helpful. The authors also thank D. Chambers, who provided the mean dynamic T/P–GRACE topography field relative to the geoid models GGM01c and GGM02c. C. King helped with the processing of T/P and Jason data. Re-analysis surface forcing fields from the National Centers for Environmental Prediction–National Center for Atmospheric Research (NCEP–NCAR) are obtained through a computational grant at NCAR. Computational support from the National Partnership for Computational Infrastructure (NPACI) and the National Center for Atmospheric Research is acknowledged. The TAF software tool was used to create the adjoint of the ECCO forward model code. This research was supported in part through ONR (NOPP) ECCO Grants N00014-99-1-1049 and N00014-99-1-1050 and through NASA Grants NAG5-11765 and NAG5-12870. This is a contribution of the Consortium for Estimating the Circulation and Climate of the Ocean (ECCO) funded by the National Oceanographic Partnership Program.

REFERENCES

Adcroft, A., J.-M. Campin, P. Heimbach, C. Hill, and J. Marshall, 2002: Mitgcm release 1. [Available online at http://mitgcm.org/sealion/.]

Birol, F., J. M. Lemoine, P. Brasseur, and J. Verron, 2005: Assimilation of satellite altimetry referenced to the new GRACE geoid estimate. *Geophys. Res. Lett.,* **32,** L06601, doi:10.1029/2004GL021329.

Chelton, D. B., J. C. Ries, B. J. Haines, L.-L. Fu, and P. S. Callahan, 2001: Satellite altimetry. *Satellite Altimetry and Earth Sciences,* L.-L. Fu and A. Cazenave, Eds., Academic Press, 1–131.

Forget, G., and C. Wunsch, 2007: Estimated global hydrographic variability. *J. Phys. Oceanogr.,* in press.

Ganachaud, A., and C. Wunsch, 2000: Improved estimates of global ocean circulation, heat transport and mixing from hydrographic data. *Nature,* **408,** 453–457.

——, ——, M.-C. Kim, and B. Tapley, 1997: Combination of TOPEX/POSEIDON data with a hydrographic inversion for determination of the oceanic general circulation. *Geophys. J. Int.,* **128,** 708–722.

Gent, P. R., and J. C. McWilliams, 1990: Isopycnal mixing in ocean models. *J. Phys. Oceanogr.,* **20,** 150–155.

Jayne, S. R., 2006: Circulation of the North Atlantic Ocean from altimetry and the Gravity Recovery and Climate Experiment geoid. *J. Geophys. Res.,* **111,** C03005, doi:10.1029/2005JC003128.

Köhl, A., Y. Lu, P. Heimbach, B. Cornuelle, D. Stammer, C. Wunsch, and the ECCO Consortium, 2002: The ECCO 1 degree global WOCE synthesis. ECCO Rep. 20, 34 pp.

——, D. Stammer, and B. Cornuelle, 2007: Interannual to decadal changes in the ECCO global synthesis. *J. Phys. Oceanogr.,* **37,** 313–337.

Large, W. G., J. C. McWilliams, and S. C. Doney, 1994: Oceanic vertical mixing: A review and a model with nonlocal boundary layer parameterization. *Rev. Geophys.,* **32,** 363–403.

LeGrand, P., H. Mercier, and T. Reynaud, 1998: Combining T/P altimetric data with hydrographic data to estimate the mean dynamic topography of the North Atlantic and improve the geoid. *Ann. Geophys.,* **16,** 638–650.

Lemoine, F., and Coauthors, 1997: The development of the NASA GSFC and NIMA Joint Geopotential Model. *Proceedings of the International Symposium on Gravity, Geoid and Marine Geodesy, IAG Symposium,* H. Fujimoto, Ed. Springer-Verlag.

Levitus, S., and T. P. Boyer, 1994: *Temperature.* Vol. 4, *World Ocean Atlas 1994,* NOAA Atlas NESDIS 4, 117 pp.

——, R. Burgett, and T. P. Boyer, 1994: *Salinity.* Vol. 3, *World Ocean Atlas 1994,* NOAA Atlas NESDIS 3, 99 pp.

Lu, Y., K. Ueyoshi, A. Köhl, E. Remy, K. Lorbacher, and D. Stammer, 2002: Input data sets for the ECCO Global 1° WOCE Synthesis. ECCO Rep. 18, 38 pp.

Olbers, D., D. Borowski, C. Völker, and J.-O. Wolff, 2004: The dynamical balance, transport and circulation of the Antarctic Circumpolar Current. *Antarct. Sci.,* **16** (4), 439–470.

Ponte, R., C. Wunsch, and D. Stammer, 2007: Spatial mapping of time-variable errors in TOPEX/POSEIDON and Jason-1 sea surface height measurements. *J. Atmos. Oceanic Technol.,* **24,** 1078–1085.

Reynolds, R. W., and T. M. Smith, 1994: Improved global sea surface temperature analyses using optimum interpolation. *J. Climate,* **7** 929–948.

Rio, M.-H., and F. Hernandez, 2004: A mean dynamic topography computed over the world ocean from altimetry, in situ measurements, and a geoid model. *J. Geophys. Res.,* **109,** C12032, doi:10.1029/2003JC002226.

Stammer, D., and Coauthors, 2002a: The global ocean circulation during 1992–1997, estimated from ocean observations and a general circulation model. *J. Geophys. Res.,* **107,** 3118, doi:10.1029/2001JC000888.

——, C. Wunsch, I. Fukumori, and J. Marshall, 2002b: State estimation improves prospects for ocean research. *Eos, Trans. Amer. Geophys. Union,* **83,** 289, 294–295.

——, and Coauthors, 2003: Volume, heat and freshwater transports of the global ocean circulation 1993–2000, estimated from a general circulation model constrained by WOCE data. *J. Geophys. Res.,* **108,** 3007, doi:10.1029/2001JC001115.

——, K. Ueyoshi, A. Köhl, W. B. Large, S. Josey, and C. Wunsch, 2004: Estimating air-sea fluxes of heat, freshwater and momentum through global ocean data assimilation. *J. Geophys. Res.,* **109,** C05023, doi:10.1029/2003JC002082.

Tapley, B. D., D. P. Chambers, S. Bettadpur, and J. C. Ries, 2003: Large scale ocean circulation from the GRACE GGM01 geoid. *Geophys. Res. Lett.,* **30,** 2163, doi:10.1029/2003GL018622.

——, and Coauthors, 2005: GGM02—An improved Earth gravity field model from GRACE. *J. Geod.,* **79,** 467–478.

Wunsch, C., 2006: *Discrete Inverse and State Estimation Problems.* Cambridge University Press, 384 pp.

——, and D. Stammer, 2003: Global ocean data assimilation and geoid measurements. *Space Sci. Rev.,* **108,** 147–162.

——, and P. Heimbach, 2006: Practical global ocean state estimation. *Physica D.,* **230,** 197–208.